RESEARCH PAPER

Thermal Analysis of a Cylindrical Heat Pipe in a Magnetic Field

Mohammadamin Soltaninejad[*], Ali Akbar Golneshan

Department of Thermo-Fluids, School of Mechanical Engineering, Shiraz University, Shiraz, Iran

Abstract

Heat pipes (HPs) are used in temperature profile flattening and cooling process of the devices involved in thermal issues. Thermal performance of a HP can be considered as a function of external and internal parameters. This research develops a numerical model with governing equations to analyze likely effects of a magnetic field on the thermal operation of a specific cylindrical HP. In this model, we consider conservation of mass, momentum, and energy, in addition to the magnetohydrodynamic (MHD) equations. We use the finite element method (FEM) to solve the system of stated equations. To demonstrate the validity of numerical results, we compare our numerical results with the results of other works in the absence of magnetic field. Additionally, we develop an experimental setup and show that our numerical and experimental results are in good agreement. Our results show that increasing the magnetic flux density from 0 to 0.2 Tesla results in three important improvements on the HP operation: (a) 47% reduction of the temperature difference, (b) reduction of the average temperature and operation pressure, and (c) increasing the uniformity of temperature distribution.

Keywords: Heat Pipe, Temperature; Heat Transfer; Fluid Flow; Magnetic Field; Magnetohydrodynamic

1. Introduction

A HP is a container inside which a working fluid transfers heat. HPs are often referred to as "superconductors" of heat due to their effectiveness in transferring high rate of heat at low temperature differences. To transfer heat in a HP, the internal working fluid is circulated between its two main sections: evaporator and condenser. Specifically, the working fluid is first evaporated in the evaporator. The produced vapor is then collected and sent to the condenser to be condensed into fresh liquid. Finally, the fluid is returned to the evaporator to be used again for transferring the heat. Phase changing of the working fluid together with the convection process has the main role in transferring the heat. In conventional HPs, the returning liquid needs a capillary force provided by a porous medium, which is called wick. A special type of wickless HPs is thermosyphon whose returning force is usually gravity [1, 2].

The development of HPs and thermosyphons has been started since about two centuries ago. An initial idea in

this field is due to Jacob Perkins [2] who invented a device for heat transfer, called Perkins tube, that its operation is similar to those of present thermosyphons. However, the principal idea of HPs was suggested by Gaugler [3], Grover [4, 5], and Cotter [6].

Numerical analysis of HPs involves a number of issues for heat transfer, fluid flow and thermodynamics [7]. One of the most important issues is coupling between velocity, temperature and operation pressure during the phase changing [8]. Reviews of HPs applications and their analysis are reported by Garimella and Sobhan [9], Carbajal [10] and Suman [11]. Xiao and Faghri [12] analyzed a chamber of HP by considering heat transfer in vapor, liquid and solid by coupling the velocity equations of the vapor and fluid. Faghri and Bucko [13] experimentally analyzed a HP for single and multiple heat sources. Furthermore, Rice and Faghri [14] numerically analyzed the prementioned case with no empirical correlations. A transient numerical analysis of a flat HP is proposed by Ranjan et al. [15]. A comprehensive review of the recent studies conducted on the HPs can be found in Ref. [16].

Recently, an important issue is attracted the attention of researchers in HP applications. That is the effect of magnetic field on the operation of HPs. The Heat transfer and fluid flow can be influenced by magnetic field. Fundamentals of magnetohydrodynamic (MHD) are described by Hosking and Dewar [17]. For detailed information on the effect of magnetic field Ref. [18, 19] could be consulted. There are a few researches for evaluation of the effects of magnetic field on the HP operation. Cingros applied a magnetic field on a Ferrofluid HP [20]. In his work temperature distribution was measured, and an increase in the Response time was observed. Cingros believed that, development of a mathematical model for such systems is complicated, therefore, he created prototypes and experimentally investigated their operations.

In another research, Aminfar et al. [21] experimentally studied the effects of applying an external magnetic field on the critical heat flux of flow boiling. Based on their results, enhancement in critical heat flux values was occurred both for pure water and Ferro fluids magnetic field imposement. For a nanofluid HP under magnetic field, Wang and Jiao [22] observed improvement of heat transfer rate in an experimental investigation. They reported that 19.2% increase could be achieved in heat flux due to both using nanofluids and magnetic field applications. Visualization of fluid flow in a pulsating HP under magnetic field was done by Kang et al. [23]. More experimental researches, were reported the effect of magnetic field on the HP operation [24-28].

As noticed, all the above-reviewed works on investigation of the effects of magnetic field on the HPs were experimental. To the best knowledge of the authors, no comprehensive numerical study has been reported yet on this issue. Specifically, none of the stated works has taken into account fluids flow, heat transfer and MHD governing equations, which are considered in a numerical analysis. In contrast to the previous studies, the present study proposes a numerical model to analyze the likely effects of magnetic field on the performance of a specific cylindrical HP. To demonstrate the validity of the proposed numerical model, an experimental test rig was developed to compare the results obtained from the numerical model and the experimental test. Results show that increasing the magnetic flux density from 0 to 0.2 Tesla results in three important improvements on the HPs operation: (a) 47% reduction in the overall temperature difference (b) lowering the average temperature as well as the operation pressure, and (c) increasing the uniformity of temperature distribution.

2. The cylindrical HP under analysis

In this section, we introduce a specific cylindrical HP in magnetic field that is heated by an electric heater and cooled in the ambient air. The general structure of this HP is shown in Fig. 1. Table 1 gives dimensions of the HP. As it is observed, the tube is made of glass and, the wick is a porous media made by sand. Seven distinguished parts are marked of Fig. 1. Parts 1, 3, 5 and 7 are the adiabatic zones. Part 2 is the evaporator that heats the HP using an electric heater. Part 4 lies between the cores of magnetic field generator, where its cross section is shown in Fig. 2. The voltage of the electrodes is 10 V. Part 6 is the condenser that is naturally cooled by atmospheric air at an ambient temperature of 21.3°C.

3. Mathematical model

The operation of the HP depends on its dimensions, its wick porosity, the rates of heat transfer in its evaporator and condenser parts, the magnetic flux density, and the material used in its construction. In this section, the governing

equations of the mathematical model of the HP's operation are described. These equations consist of MHD equations, mass conservation, momentum conservation, energy conservation, and some additional equations of heat transfer, mass transfer and phase changing. The governing equations for the three parts of the HP, i.e., the wall (tube), wick and vapor domains are as follows (more details can be found in Ref. [8, 29, 30]).

Let ρ_e be the electric charge density. Furthermore, let $\mathbf{E}$, $\mathbf{B}$ and $\mathbf{J}$ denote the vectors of electric field strength, magnetic flux density, and current density, respectively. Then the Lorentz force $\mathbf{F}_b$, which is the MHD force exerted due to the magnetic field is defined as follows [31]:

$$\mathbf{F}_b = \rho_e \mathbf{E} + \mathbf{J} \times \mathbf{B} . \tag{1}$$
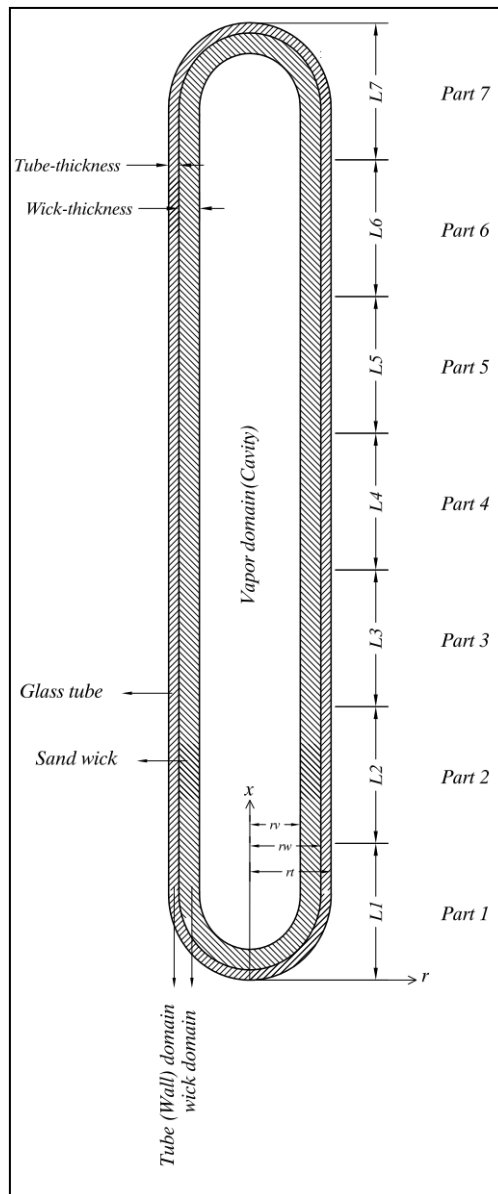
Fig. 1 General structure of the HP under analysis

Table 1 Dimensions of the HP under analysis

Axial length [mm]

L1	L2	L3	L4	L5	L6	L7
30	120	110	50	110	120	30

Radius [mm]		
r_v	r_w	r_t
6	9	11
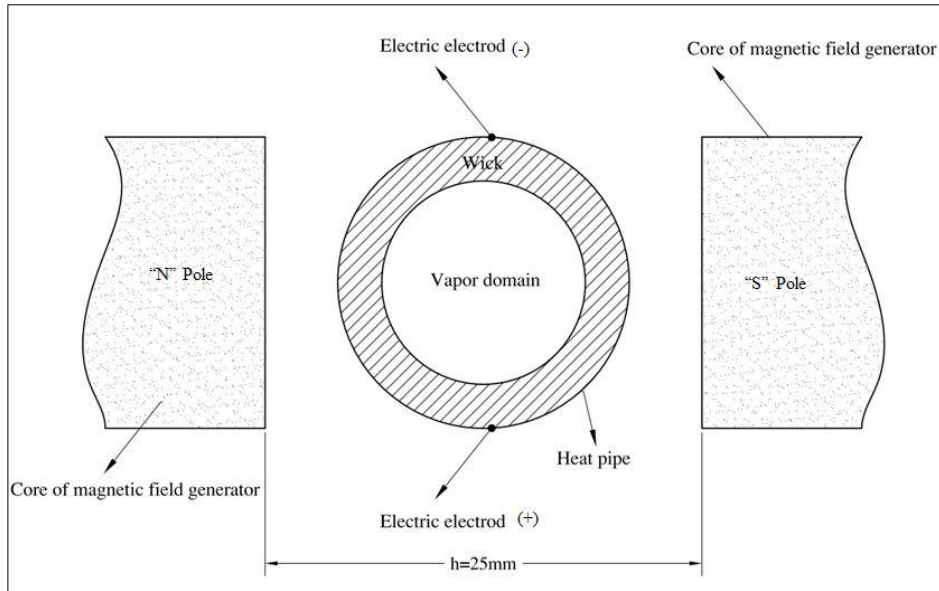
Fig. 2 Cross section of part 4 of the HP under analysis

To calculate the terms of the Lorentz force, we need three equations of Maxwell (i.e., Gauss's law, Faraday's law and Ampere-Maxwell's law), Ohm's law and current conservation equation [32]. The Gauss's law is defined by

$$\nabla \cdot \mathbf{E} = \frac{\rho_e}{\varepsilon_0}, \tag{2}$$

where ∇ and ε_0 are divergence operator and the vacuum permittivity (that its value in SI is $8.85 \times 10^{-12} [F.m^{-1}]$), respectively. The Faraday's law is defined as

$$\nabla \times \mathbf{E} = -\frac{\partial \mathbf{B}}{\partial t}, \tag{3}$$

where t is the time. The Ampere-Maxwell's law is given by

$$\nabla \times \mathbf{B} = \mu_0 \mathbf{J} + \mu_0 \varepsilon_0 \frac{\partial \mathbf{E}}{\partial t}, \tag{4}$$

where μ_0 is the vacuum permeability and its value in SI is $4\pi \times 10^{-7} [H.m^{-1}]$.

The current conservation equation is given by

$$\nabla \cdot \mathbf{J} = -\varepsilon_0 \frac{\partial}{\partial t} \nabla \cdot \mathbf{E}, \tag{5}$$

which is simplified using the Gauss's law as follows:

$$\nabla \cdot \mathbf{J} = -\frac{\partial \rho_e}{\partial t} \ . \tag{6}$$

Let σ be the electrical conductivity. The Ohm's law is defined as the following equality:

$$\mathbf{J} = \sigma \left(\mathbf{E} + \mathbf{u} \times \mathbf{B} \right), \tag{7}$$

Where $\mathbf{u}$ denotes velocity vector. The notation φ shows the porosity stating the volume of the voids in the porous media per total volume of the media [29]:

$$\varphi = \frac{volume_{\text{void}}}{volume_{\text{total}}} \ . \tag{8}$$

The value of φ is 0 for the tube domain, 1 for the vapor domain, and 0.39 for the wick domain where is measured by a test.

Darcy's law in porous medium is given by:

$$\mathbf{u} = (-\nabla P)(\frac{K}{\varphi \mu}), \tag{9}$$

where P, K and μ are pressure, permeability of the porous medium and dynamic viscosity of the fluid, respectively.

Let ρ and g denote density and gravitational acceleration. The subscripts "r" and "x" indicate the coordinates (see Fig.1). The continuity equation for the vapor and wick domains is

$$\frac{1}{r}\frac{\partial}{\partial r}(\rho r u_r) + \frac{\partial}{\partial z}(\rho u_x) + \varphi \frac{\partial \rho}{\partial t} = 0 \ . \tag{10}$$

The momentum equations for the vapor and wick domains for the directions r and x are given, respectively, by

$$\begin{aligned}
&\frac{\partial}{\partial t}(\rho u_r) + \frac{\partial}{r\partial x}(r\rho u_x u_r) + \frac{\partial}{r\partial r}(r\rho u_r u_r) + \varphi \frac{\partial P}{\partial r} = \frac{1}{r}\frac{\partial}{\partial x}\left[r\mu\left(\frac{\partial u_x}{\partial r} + \frac{\partial u_r}{\partial x}\right)\right] \\
&+ \frac{1}{r}\frac{\partial}{\partial r}\left[r\mu\left[2\frac{\partial u_r}{\partial r} - \frac{2}{3}\left(\frac{\partial}{\partial x}(u_x) + \frac{\partial}{r\partial r}(ru_r)\right)\right]\right] - 2\mu \frac{u_r}{r^2} + \frac{2}{3}\frac{\mu}{r}\left(\frac{\partial}{\partial x}(u_x) + \frac{\partial}{r\partial r}(ru_r)\right) + \rho\frac{u_x^2}{r} + F_{w_r} + F_{b_r},
\end{aligned} \tag{11}$$

and

$$\begin{aligned}
&\frac{\partial}{\partial t}(\rho u_x) + \frac{\partial}{r\partial x}(r\rho u_x u_x) + \frac{\partial}{r\partial r}(r\rho u_r u_x) + \varphi \frac{\partial P}{\partial x} = \\
&\frac{1}{r}\frac{\partial}{\partial x}\left[r\mu\left[2\frac{\partial u_x}{\partial x} - \frac{2}{3}\left(\frac{\partial}{\partial x}(u_x) + \frac{\partial}{r\partial r}(ru_r)\right)\right]\right] + \frac{1}{r}\frac{\partial}{\partial r}\left[r\mu\left(\frac{\partial u_x}{\partial r} + \frac{\partial u_r}{\partial x}\right)\right] + \rho g + F_{w_x} + F_{b_x},
\end{aligned} \tag{12}$$

where F_{w_r} and F_{w_x} are the source terms due to fluid flow in the porous media, also, F_{b_r} and F_{b_x} are the two components of Lorentz force in the r and x directions, respectively.

Let d be the diameter of the particles in the porous media. Then the permeability of the wick, denoted by K, is defined as follows [33, 34]:

$$K = \frac{d^2 \varphi^3}{150(1-\varphi)^2} \ . \tag{13}$$

With $d = 0.7[mm]$ and $\varphi = 0.39$, K is equal to $5.2 \times 10^{-10}[m^2]$. Let C_E denote the Ergun's Coefficient. It is a

function of shape factors of the particles of the wick. That is assumed to be equal to 0.237 [35]. The subscript "*w*" indicates the wick domain, and the subscript "*l*" the liquid in the wick domain. Then, the source forces on the liquid in the wick, in the directions *r* and *x* are written, respectively, as

$$F_{w_r} = -\frac{C_E \varphi \rho_l \left|\mathbf{u}\right|}{\sqrt{K}} u_{l_r} - \frac{\mu_l \varphi}{K} u_{l_r}, \tag{14}$$

$$F_{w_x} = -\frac{C_E \varphi \rho_l \left|\mathbf{u}\right|}{\sqrt{K}} u_{l_x} - \frac{\mu_l \varphi}{K} u_{l_x}. \tag{15}$$

Here, the first terms of F_{w_r} and F_{w_x} are the inertial terms, and their second terms are the viscous terms. Let k_s and k_l denote thermal conductivities of solid and liquid phases in the wick, respectively.

Then the thermal conductivity of the wick, k_w, could be determined as [36]:

$$k_w = \frac{k_l \left[k_l + k_s - (1-\varphi)(k_l - k_s)\right]}{(k_l + k_s) + (1-\varphi)(k_l - k_s)}. \tag{16}$$

Let c_p and T denote the specific heat capacity and temperature, and the subscripts "*t*" and "*v*" indicate tube and vapor domains, respectively. The energy conservation equations for the tube, vapor and wick domains are, respectively, as follows:

$$\left(\rho c_p\right)_t \frac{\partial T}{\partial t} = k_t \left[\frac{1}{r}\frac{\partial}{\partial r}\left(r\frac{\partial T}{\partial r}\right) + \frac{\partial^2 T}{\partial x^2}\right], \tag{17}$$

$$\left(\rho c_p\right)_v \frac{\partial T}{\partial t} + \frac{\partial}{r\partial r}\left(\left(\rho c_p\right)_v \left(ru_r T\right)\right) + \frac{\partial}{\partial x}\left(\left(\rho c_p\right)_v \left(u_x T\right)\right) = k_v \left[\frac{1}{r}\frac{\partial}{\partial r}\left(r\frac{\partial T}{\partial r}\right) + \frac{\partial^2 T}{\partial x^2}\right], \tag{18}$$

$$\left[\left(\rho c_p\right)_w\right]\frac{\partial T}{\partial t} + \frac{\partial}{r\partial r}\left(\left(\rho c_p\right)_l \left(ru_r T\right)\right) + \frac{\partial}{\partial x}\left(\left(\rho c_p\right)_l \left(u_x T\right)\right) = k_w \left[\frac{1}{r}\frac{\partial}{\partial r}\left(r\frac{\partial T}{\partial r}\right) + \frac{\partial^2 T}{\partial x^2}\right]. \tag{19}$$

In the HP under analysis, there are five terms of pressure head that are balanced as

$$\Delta P_{MHD} + \Delta P_c + \Delta P_g = \Delta P_v + \Delta P_w, \tag{20}$$

where ΔP_{MHD}, ΔP_c and ΔP_g are the pumping heads of magnetic field, capillary and gravity forces, respectively. Furthermore, ΔP_v and ΔP_w are the pressure losses of the fluid flow in the vapor and wick domains, respectively.

4. Boundary conditions
By the prementioned equations in the previous section, solving the problem is possible, if the boundary conditions (B.C.s) exist. Based on Fig. 1 the B.C.s of the domains are defined. In the outer layer of the HPs, there are three types of B.C.s as follows:

1) **Adiabatic or insulated parts:** for parts 1, 3, 5 and 7, we need to impose the following equality:

$$-k_t \left[\frac{dT}{dr}\right]_t = 0. \tag{21}$$

2) **Constant heat flux in the evaporator section:** for part 2, then the B.C is as follows:

$$-k_t \left[\frac{dT}{dr}\right]_t = q''. \tag{22}$$

where q'' denotes the heat flux.

3) **Convection in parts 4 and 6:** these parts are in the ambient air, hence, we need to impose the following equality:

$$-k_t \left[\frac{dT}{dr}\right]_t = h_{conv}(T - T_{ambient}) .$$ (23)

In the interface boundary of the wick and the tube domain, there is no mass transfer. The only Heat transfer mechanism in this boundary is just heat conduction. So, the conditions of this boundary are as follows:

$$-k_t \left[\frac{dT}{dr}\right]_t = -k_w \left[\frac{dT}{dr}\right]_w ,$$ (24)

$$\mathbf{u} = 0 .$$ (25)

There are mass transfer and phase changing in the interface boundary of the wick and vapor domains. Let $\bar{m}''$ and h_{fg} denote the mass flux and latent heat, respectively. So, the B.C.s can be assumed as follows:

$$u_1 = \frac{\bar{m}''}{\rho_1} ,$$ (26)

$$u_v = \frac{\bar{m}''}{\rho_v} ,$$ (27)

$$-k_w \left(\frac{\partial T}{\partial r}\right)_w = -k_v \left(\frac{\partial T}{\partial r}\right)_v + \bar{m}'' h_{fg} .$$ (28)

5. Numerical solutions

Using the governing equations and boundary conditions, a numerical solution is considered. Finite element method (FEM) is used to discrete the governing equations. The equations are solved coupled and simultaneously. Also, an average of the magnetic force on the circle circumference cross section of the HP is used. To the best convergence in solving process, the following three steps are considered:

Step 1 Modeling the HP, assuming the wick is filled by liquid and ignoring the porous media, in the absence of any magnetic field,

Step 2 Modeling the HP, considering the porous media in the wick but no magnetic field,

Step 3 Modeling the HP, considering the porous media in the wick and applying the magnetic field (full model).

In the solution, it is assumed that:

- the vapor and liquid flow are compressible (Mach<0.3)
- the operation is in the steady state condition
- viscous dissipation is negligible (due to low velocities)
- vapor is an ideal gas
- the wick is saturated with liquid (the wick domain is just filled by liquid and the cavity domain is filled by vapor)
- radiation heat transfer is negligible

Using Eq. (27), the interface temperature of wick and vapor domain (T_i) can be calculated, also, its corresponding pressure (P_i) can be evaluated by Clausius-Clapeyron equation, as follows [37]:

$$P_i = P_{ref} \exp\left[\left(\frac{h_{fg}}{R}\right)\left(\frac{1}{T_{ref}} - \frac{1}{T_i}\right)\right],$$ (29)

where, P_{ref} and T_{ref} denote the reference values and can be evaluated from thermodynamic tables for saturated water. In this research, $P_{ref} = 3160[Pa]$ and $T_{ref} = 298[K]$ are assumed. Furthermore, R denotes the gas constant.

Let α denote the accommodation coefficient. It is set to be 0.035 in this study based on Ref. [38]. The mass flux in this interface boundary ($\bar{m}''$) can be extracted by kinetic theory [39-41]

$$\bar{m}'' = \left(\frac{2\alpha}{2-\alpha}\right)\left(\frac{1}{\sqrt{2\pi R}}\right)\left(\frac{P_v}{\sqrt{T_v}} - \frac{P_i}{\sqrt{T_i}}\right). \tag{30}$$

The sign of $\bar{m}''$ in the above equation is the criterion to determine which of the condensation or evaporation process is occurred in the phase changing. Based on this equation, if $P_v/\sqrt{T_v}$ is greater than $P_i/\sqrt{T_i}$, then $\bar{m}''$ will be positive, it means condensation of the vapor is happened. On the contrary, being $P_i/\sqrt{T_i}$ greater than $P_v/\sqrt{T_v}$, makes the $\bar{m}''$ negative, so, evaporation of the liquid is happened.

In the numerical solution, the pressure in the HP is divided into two parts

$$P = P_M + P_O, \tag{31}$$

where the first term (P_M) is the momentum pressure, which is a function of location and in the solution process is calculated by momentum conservation equation. Furthermore the second term (P_O) is the operation pressure. It is just time dependent. This pressure does not change with location and can be calculated by the ideal gas assumption, as follows:

$$P_O = m_v R \sum_{vapor}\left(\frac{T_v}{V_v}\right). \tag{32}$$

The temperature dependency of the latent heat h f g is defined as follows [37]:

$$h_{fg} = 3372.6 - 5.7223T + .0115T^2 - .00001T^3 . \tag{33}$$

Electric and magnetic properties of the liquid are listed in Table 2. Thermo-Physical properties of the materials are listed in Table 3. The problem is steady-state, but to consider the temperature differences and for better convergence in the solution process, the properties are considered as a function of temperature.

6. Experimental setup

In this section, we describe how the HP under analysis is manufactured and magnetic field generator is described. Then, we introduce the used devices and their arrangement in the experimental setup.

Based on Fig. 1 the structure of the HP is manufactured. Rounded glass and wick at the both ends of the HP are ignored. Because non-condensable gases make bad effects on the operation of any HP, we evacuate the HP under analysis as shown in Fig. 3 (item 1), so that these gases are extracted from the HP, using the vacuum pump (item 2), a pressure gauge is used (item 3) to measure the pressure, and the working fluid is rather injected inside the HP from the storage tank (item 4). Water is used as the working fluid. To control the manufacturing process, four valves (item 5) are installed in the piping paths. The process is completed by sealing the HP. The model of the pressure gauge (item 3) is Pfeiffer (model TPR 280) and its accuracy for pressure ranges of this research is 3 mbar.

Fig. 4 shows the manufactured generator of magnetic field and explains how the HP is installed in the gap created in the core of this generator. As can be seen, the generator consists of two solenoids and one core. The magnetic flux density is adjustable from 0 to 0.25 Tesla in this generator. We use three magnetic flux densities 0, 0.1 and 0.2 Tesla in the tests and simulations ($\mathbf{B} = 0, 0.1$ T, 0.2 T).

Table 2 Electric and magnetic properties of the liquid [42, 43]

Relative permittivity	Relative permeability	Electrical conductivity [S/m]
80.0	1.0	0.1

Table 3 Thermo-Physical properties of the used materials [44, 45]

	Thermal conductivity [W/m.k]	Viscosity [Pa.s]
Glass	1.8	---
Water liquid	$-0.7522 + .0074T - (1e-5)T^2$	$3.82e-2/(T-252.33)$
Water vapor	$-(1.39e-2) + (1.01e-4)T$	$-(3.09e-6) + (4.07e-8)T$
Sand	$1.241 + .006T$	---
Air	$.0003 + (9e-5)T - (3e-8)T^2$	$(2e-6) + (6e-8)T - (2e-11)T^2$
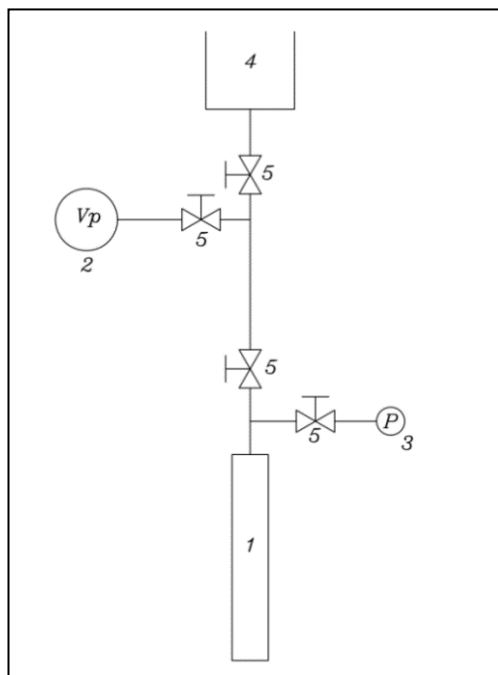
Fig. 3 Proposed piping system for construction of the HP under analysis
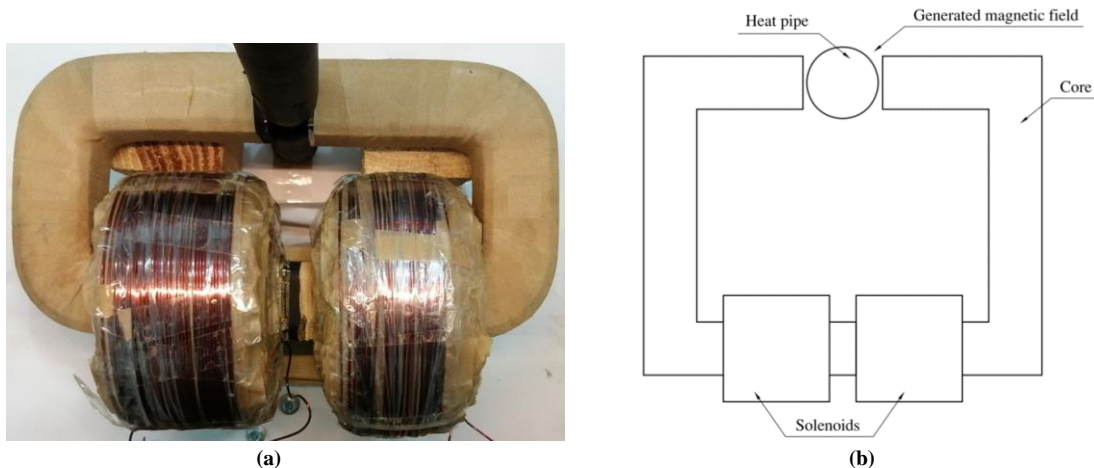
Fig. 4 Magnetic field generator ((a) The generator of magnetic field used in the experimental setup (b) Installing the HP under analysis in the magnetic field)

Fig. 5 shows the experimental setup and introduces the devices used in the experiment and their arrangement. The stated devices are the followings:

1) Solenoids of the magnetic field generator
2) Core of the magnetic field generator
3) DC power suppliers for the magnetic field generator
4) HP
5) Electric heater in the evaporator section (the outer side of the heater is insulated)(Q=5 W)
6) Power supplier for the electric heater
7) Voltage regulator
8) Electric circuit
9) Power supplier
10) Cooling fan for core and solenoids

To start the experiments, heat is first applied at the evaporator part. The working fluid circulation is started, under the effect of magnetic field, gravity and capillary forces. The condenser part is cooled at the room temperature (21.3°C). Temperature values are measured by pt100 sensors that are installed in the outer wall and inside of the HP. The measurement accuracy is ±0.2°C. The operation pressure is measured by the pressure gauge.

7. Results and Discussion

In this section, the results obtained from the experimental and numerical tests are discussed. To demonstrate the validity of the numerical solution (in the presence of working fluid in the porous media of the HP and in the absence of magnetic field), we compare our results with those of Faghri and Bucko [13] and Rice and Faghri [14]. In these two works, the values of r_t, r_w and r_v are assumed as 12.7, 11 and 10.25 mm, respectively. The total length of the HP is 1000 mm, the length of the evaporator is 63.5 mm, the condenser length is 300 mm and the other parts are in adiabatic condition. The comparison is done for power input of 90 W.

This comparison is shown in Fig. 6. As can be observed, there is a good agreement between the results. The effects of magnetic field on the temperature distribution, velocity profiles of working fluid, pressure distribution and heat transfer in the HP are examined. The results of the numerical solution are compared to the present experimental results. The results are presented in following.
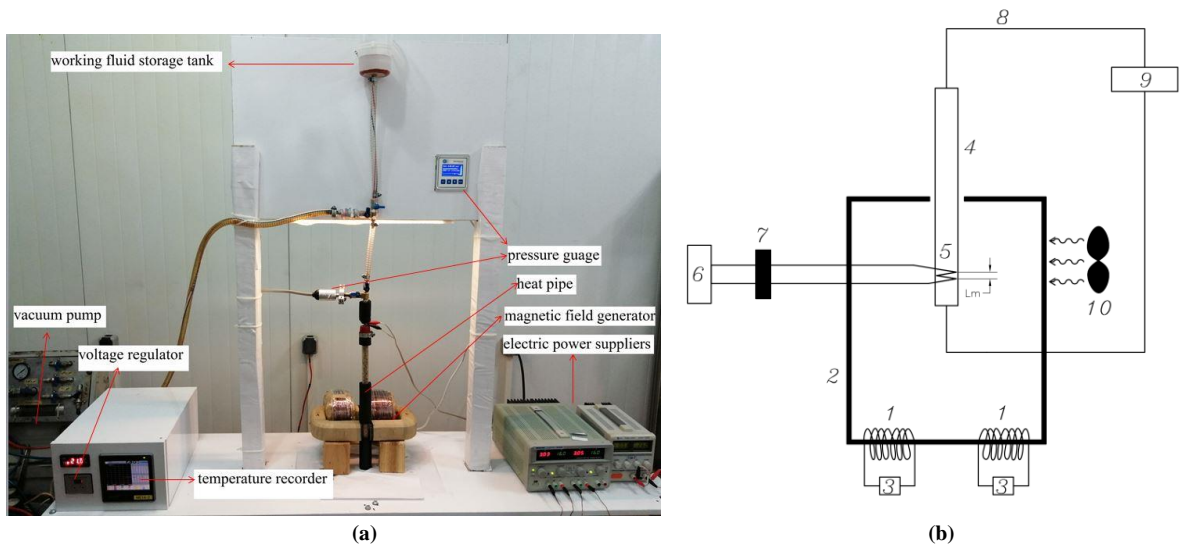
Fig. 5 Arrangement of the experimental setup ((a) Real photo (b) schematic))
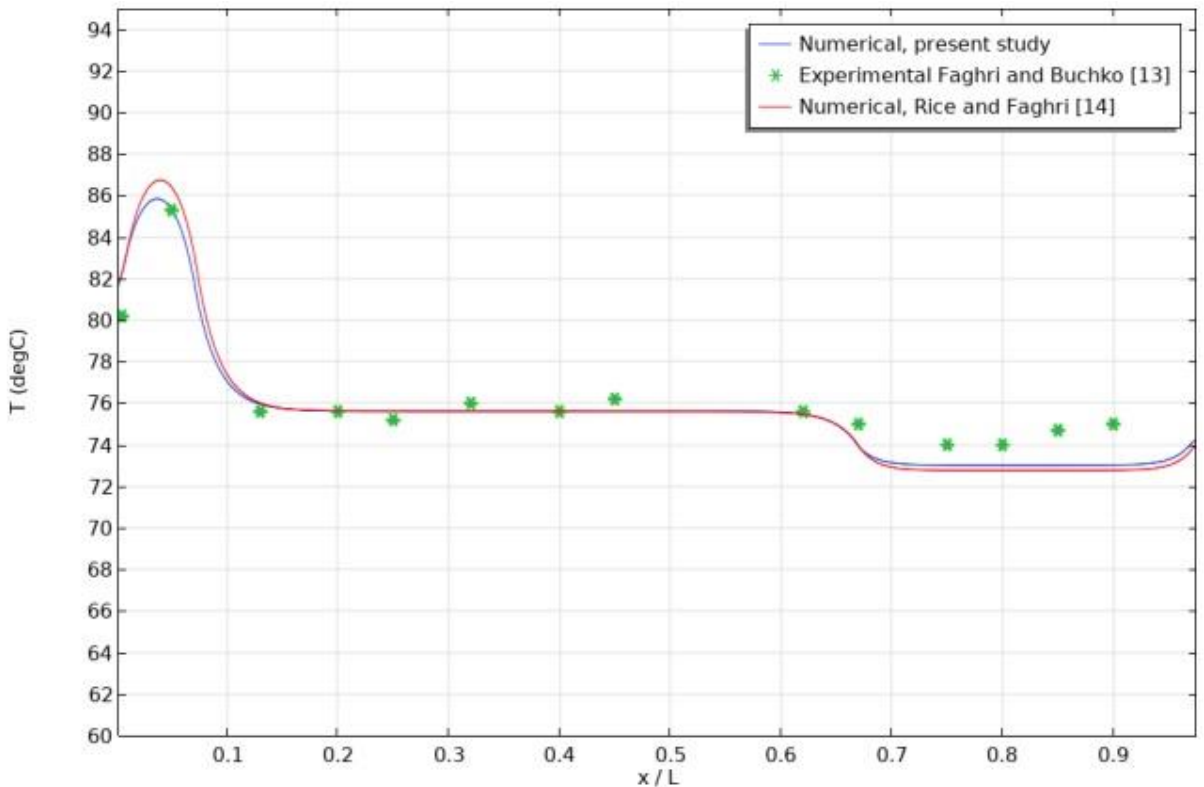
Fig. 6 Comparison of the results with the results of Faghri and Bucko [13] **and Rice and Faghri.**[14]

7.1 The heat transfer ability of the HP under analysis

In this subsection, two cases are considered: The first, modelling a HP without any working fluid and the second, a HP containing a working fluid. Both HPs are checked. Temperature contours of both HPs are shown in Fig. 7, and temperature distributions along the axis of the HPs are shown in Fig 8.

It is observed that the temperature on the axis of the HP gets more uniform in the presence of the working fluid.

From Fig. 7 and Fig. 8 it is observed that presence of the working fluid leads to reducing the maximum temperature from 1080 to 92.5°C as well. The temperature difference along the HP is reduced from 1060 to 7.5°C. This considerable improvement of temperature difference reduction is due to the circulation and phase changing of the working fluid, confirming the HP ability in transferring heat.

7.2. Effects of magnetic field on the velocity profiles in the HP

Fluid flow in HPs which dictates the operation of the HP, is affected by parameters like: power input in the evaporator, condenser conditions, adiabatic section conditions, material of the working fluid, wick porosity; HP geometry, and external forces. In this subsection the effects of magnetic flux density on the velocity is shown. Circulation of the fluid in the HP consists of two parts:

• Vapor flow in the vapor domain,
• Liquid flow in the wick.

For the presented model, the fluid flow is shown in Fig. 9. Based on this figure, liquid in the wick is moving down from the condenser to the evaporator part, then it is evaporated in the bottom section of the HP (the evaporator), and the evaporated fluid moves to the top and is condensed in the condenser. The velocity vectors are magnified and normalized for better clarity.

(a)　　　　　　　　　　　　　　　　(b)
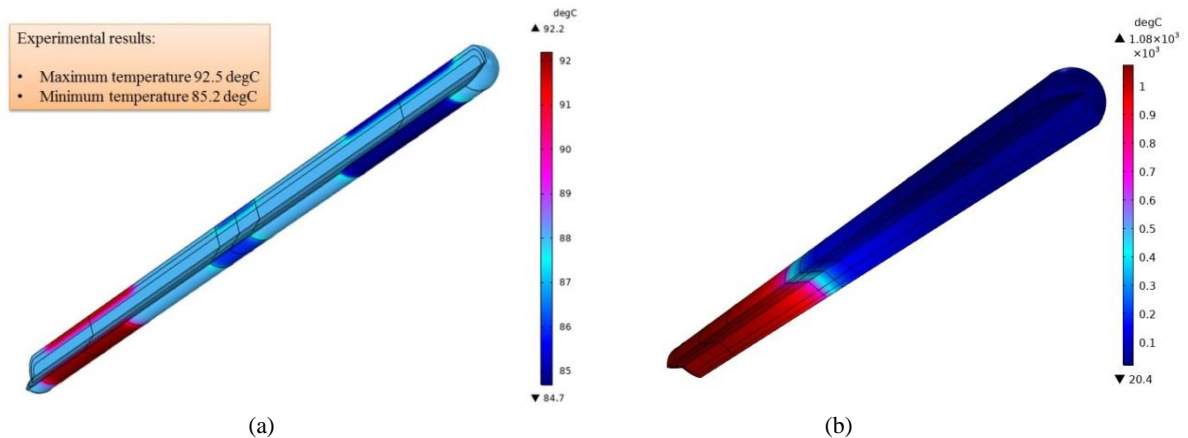
Fig. 7 Temperature profiles along the HP ((a) With working fluid (b) Without working fluid))

(a)　　　　　　　　　　　　　　　　(b)
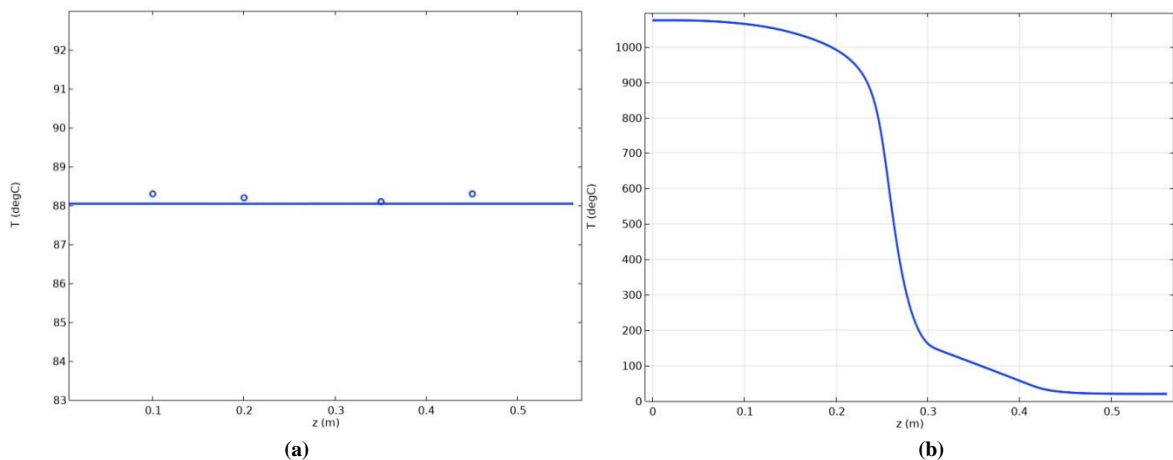
Fig. 8 Temperature distributions along the axis of the HP ((a) With working fluid (b) Without working fluid))
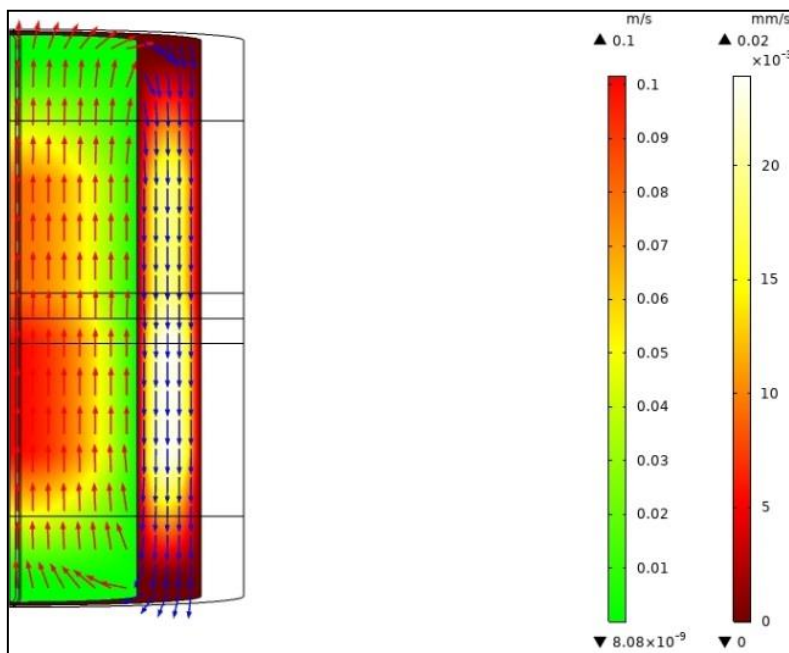
Fig. 9 Fluids flow through the HP

Fig. 10a shows the radial velocity of vapor at $x = L_1 + L_2 + L_3$. The maximum velocity is on the centerline of the HP and it is decreased to the zero value at the edge of the vapor domain. Based on this figure, by increasing the magnetic flux density, the vapor velocity will be increased, showing the effect of external force exerted by magnetic field. The velocity contour of the vapor domain for different magnetic flux densities is shown in Fig. 10b-10d. Because of evaporation and condensation along the HP, the velocity in the middle of the HP is larger than the top or bottom parts.

In Fig. 11a absolute value of liquid axial velocity in the wick is shown (for 8.15 mm $< r < 8.40$ mm). Furthermore, in Fig. 11b the contour of this velocity is shown. By changing the magnetic flux density, the variations of the liquid velocity in the wick are small, because of the low velocity values of the liquid. The radial velocity of the vapor profile on the common boundary of the wick and the vapor domains and its contour is shown in Fig. 12. In this figure, negative velocity indicates the evaporation, it means that the vapor is generated and entered in the vapor domain, on the contrary, positive velocity indicates the condensation. It is observed that condensation and evaporation rates are increased as the magnetic flux density is increased.

Note that in all the above mentioned velocity contours, the dimensions of the HP are magnified for better clarity.

(a) For different B values   **(b)) B=0.2 T**

(c) B=0.1 T   **(d) B=0**
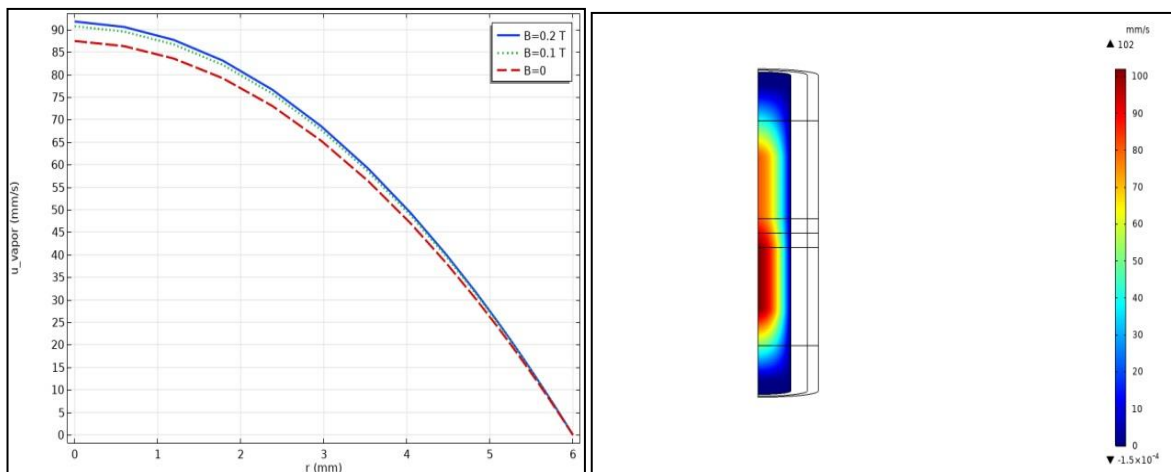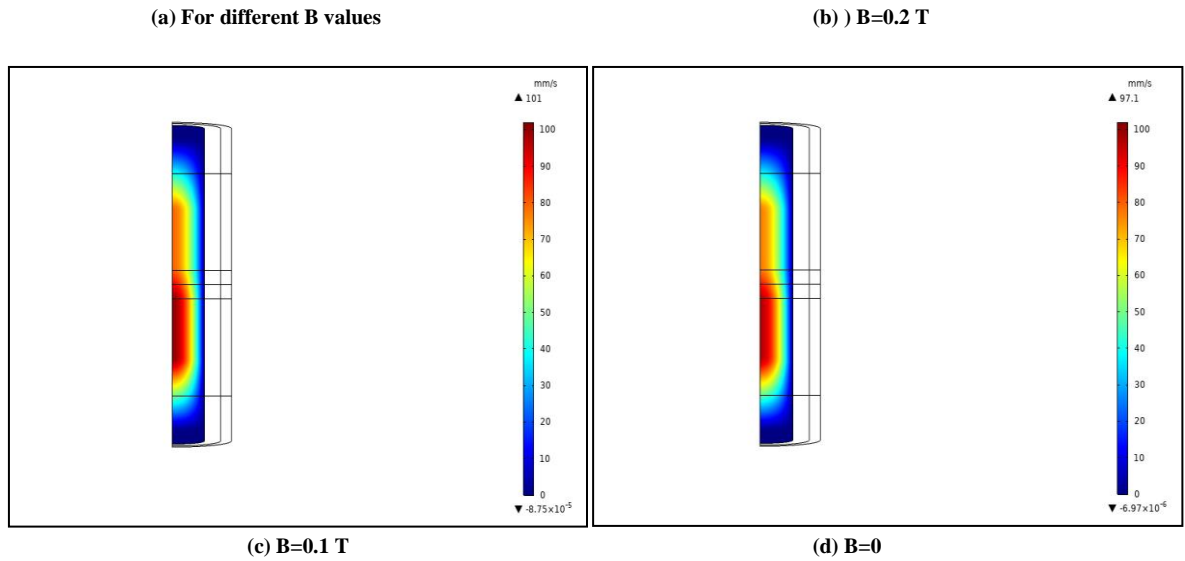
Fig. 10 Axial velocity for the vapor phase through the HP
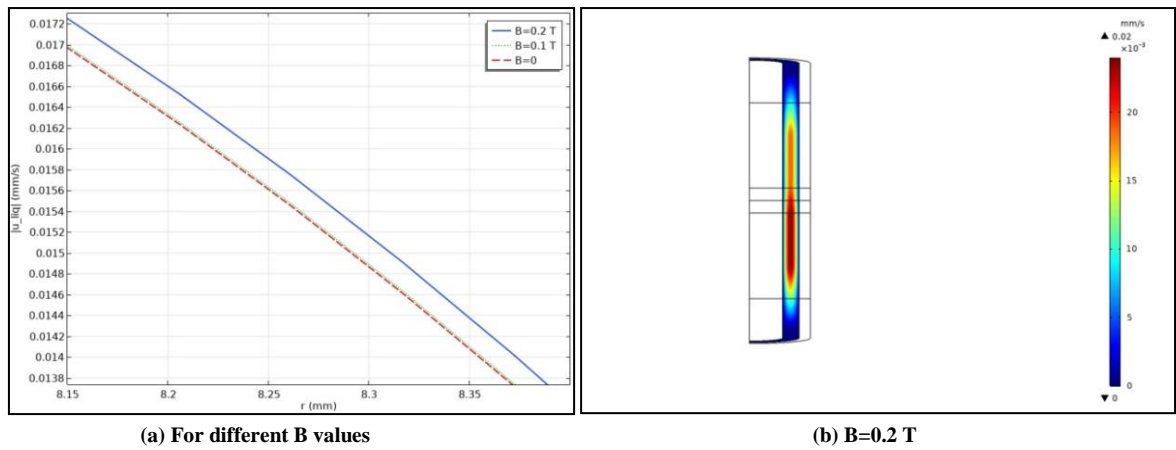
(a) For different B values   **(b) B=0.2 T**
Fig. 11 Absolute value of axial velocity for the liquid phase through the wick of the HP
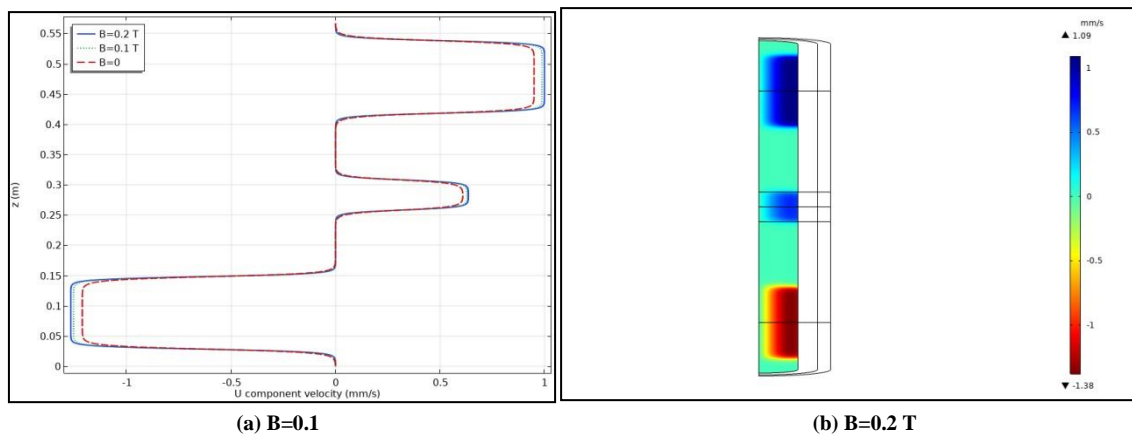
(a) B=0.1   **(b) B=0.2 T**
Fig. 12 Radial velocity for the vapor phase along the HP on the wick-vapor boundary

7.3 Effects of magnetic field on the temperature distribution in the HP

Fig. 7a and Fig. 13 show the temperature contours and Table 4 shows the temperature parameters for different magnetic flux densities. They show that, the temperature distribution gets more uniform along the HP by applying and

increasing the magnetic flux density.

By increasing **B** from 0 to 0.2 T, the temperature difference along the HP, is reduced from 7.5°C to 4°C (47% reduction), furthermore, the maximum temperature is reduced from 92.2°C to 88.9°C. Also, it is shown that, the average temperature of the HP is reduced in the presence of magnetic field. This is due to higher vapor velocities along the HP, as declared by Fig 10. This effect was also explained in the previous subsection.

(a) B=0.1 T   (b) B=0.2 T
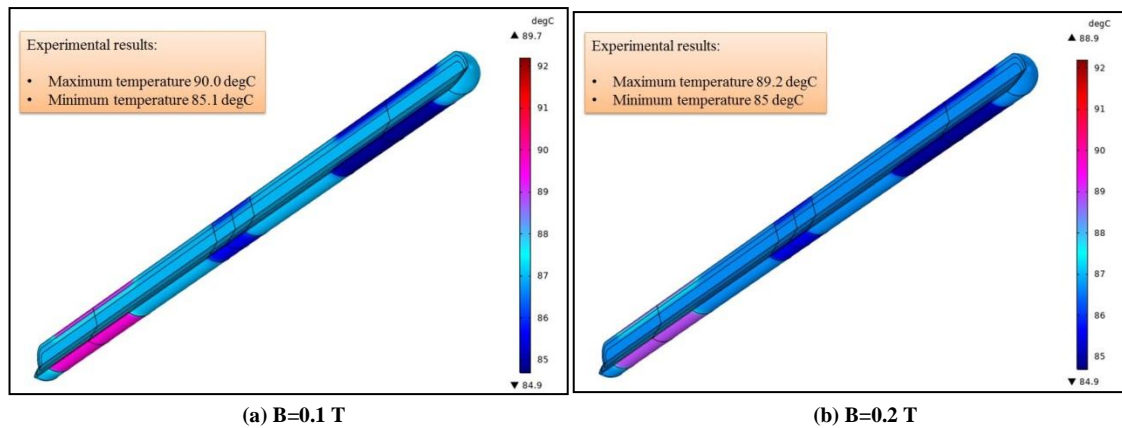
Fig. 13 Temperature contours of the HP for different B values

Table 4 Temperature parameters for different B values

	Magnetic flux density [T]		
	B=0	B=0.1	B=0.2
Maximum temperature in the HP (degC)	92.2	89.7	88.9
Average temperature in the HP (degC)	88.1	86.9	86.6
Minimum temperature in the HP (degC)	84.7	84.9	84.9
temperature gradient in the HP (degC)	7.5	4.8	4.0
Appearance thermal conductivity (W/(m.K))	997.8	1561.7	1890.8

By reversing the direction of the magnetic field, the magnetic force is the force resisting the working fluid flow in the HP, so the temperature of the HP would be increased. Temperature contours of the HP are shown in Fig 14 for the reversed magnetic field direction.

By defining "apparent conductivity" as: the heat transferred in the HP over the temperature gradient along the HP, it is shown that the apparent thermal conductivity is increased about 89% (from 997.8 to 1890.8 W.m^{-1}.K^{-1}) by increasing **B** from 0 to 0.2 T.

Fig. 15 shows the temperature profile in the evaporator part of the HP, at $x = L_1 + L_2 / 3$. Based on this figure, in the r-direction, the temperature is not much different in the vapor domain (from r = 0 to 6 mm), however, it is increased across the wick thickness (from r = 6 to 9 mm) and across the tube thickness (from r = 9 to 11 mm) due to thermal resistance of these domains. The temperature profile in the r-direction becomes flatter by increasing the magnetic flux density. The temperature values are also lowered by this effect.

Fig. 16 shows the temperature distribution along the axis through the HP. It is seen that the temperature along the axis is approximately uniform, this is due to high vapor velocity in this region. If the magnetic flux density increases from 0 to 0.1 Tesla, the average temperature is reduced from 88.1°C to 86.9°C, and in case of B=0.2 T this temperature is reduced to 86.6°C.

Fig. 17 shows the temperature distribution along the outer surface of the HP for different magnetic flux densities. It is observed that the highest temperature for a specified magnetic flux density is located on the evaporator and the lowest on the condenser. Close agreements are observed between the experimental data and the simulated results. The small mismatch could be the result of many parameters, among them a few but not all are: the presence of small amount of non-condensable gases in the HP, accuracy of the measuring tools, simplifications made in the numerical simulation and etc.
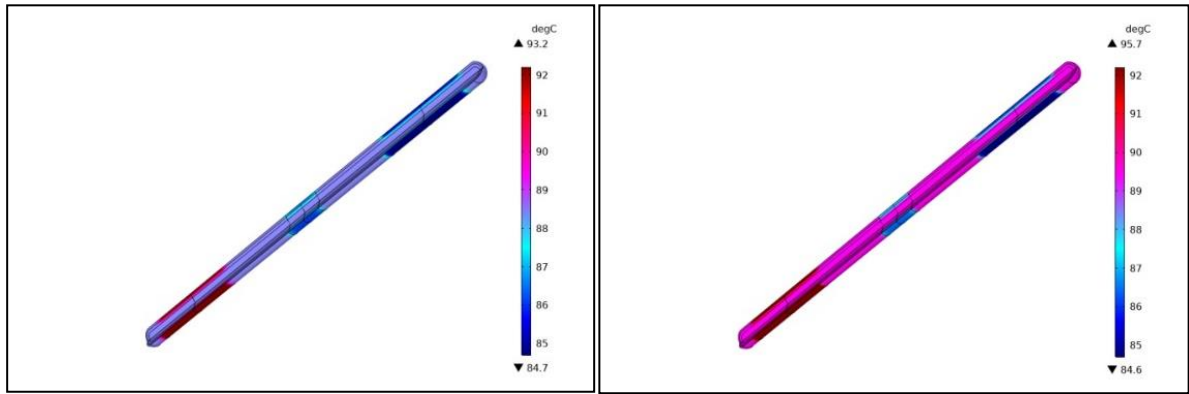
(a) B=0.1 T   (b) B=0.2 T

Fig. 14 Temperature contours of the HP for reversed direction of different B values
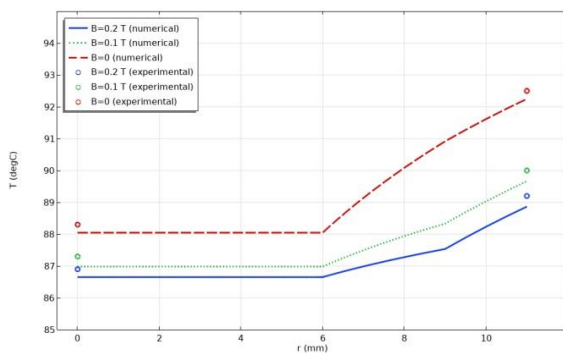
Fig. 15 Radial temperature distributions in the evaporator section for different B values
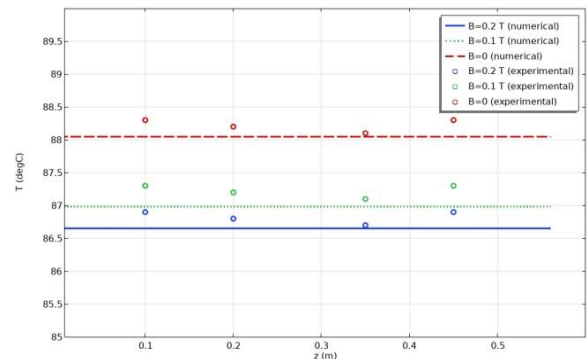
Fig. 16 Vapor temperature profiles for different B values along the axis of the HP

7.4. Effects of magnetic field on the pressure distribution in the HP

Based on the prementioned governing equations, the pressure in the HP is composed of two parts: momentum pressure (P_M) and operation pressure (P_O). In Fig. 18 the momentum pressure contour in the wick is shown for **B**=0.2 T. The dimensions of the HP are magnified 20 times in r-direction for more clarity.

It is seen that the momentum pressure is changed from 1.96 kPa in the condenser to -1.96 kPa in the evaporator. The magnetic field, gravity and porosity in the wick are responsible for this pressure gradient. In table 5 the operation pressure in the HP for different magnetic flux densities is shown. Increasing the magnetic flux density enhances the fluid flow and heat transfer in the HP, resulting in the reduction of the average temperature and the operation pressure, because the operation pressure is a function of temperature, as discussed in Eq. (31). In this table results of both experimental work and numerical simulation are tabulated. Good agreement is observed.

7.5. Effects of magnetic field on heat transfer and energy balance in the HP

To show the heat transfer mechanism in the HP, a resistance network is considered as shown in Fig. 19. The heat transferring can be decomposed into two parts: Q_1 and Q_2. The Q_1 is the major part of the transferred heat in the HP, due to the convection and phase changing. The Q_2 is heat losses along the HP. The transferred heat in the HP for each part is shown in Table 6. Based on this table more than 99% of the heat is Q_1. By applying a magnetic field on the HP,

the convection term becomes greater such that the percentage of the transferred heat Q_1 is increased.
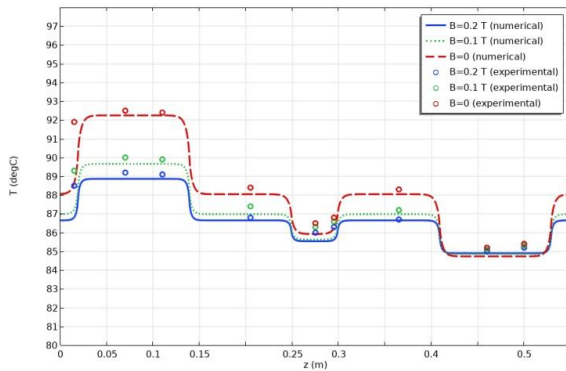
Fig. 17 Temperature profiles for different B values along the outer side of the HP
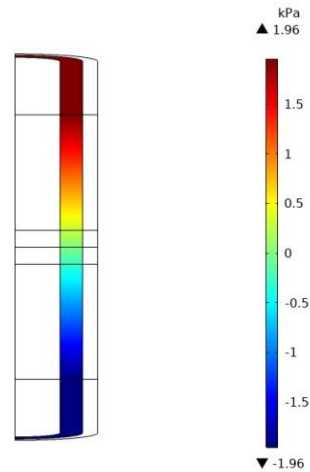
Fig. 18 Momentum pressure contour through the wick of the HP for B = 0.2 T

Table 5 Operation pressure of the HP for different B values [kPa]

	Magnetic flux density [T]		
	B=0	B=0.1	B=0.2
Numerical	65.59	63.01	62.23
Experimental	65.77	63.04	62.07

Table 6 Details of heat transfer process in the HP for different B values

	Magnetic flux density [T]		
	B=0	B=0.1	B=0.2
Input power [W]	5.000	5.000	5.000
Q_1 [W]	4.956	4.963	4.965
Percentage of Q_1	99.12	99.26	99.30
Q_2 [W]	0.044	0.037	0.035
Percentage of Q_2	0.88	0.74	0.70
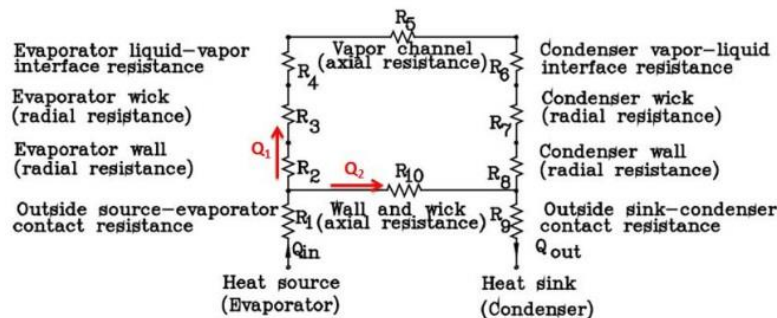
Fig. 19 Thermal resistance network of the HP [16]

8. Conclusions

This research investigated the likely effects of magnetic field on the operation of a specific cylindrical HP from both numerical and experimental points of view. Based on the analysis, the following conclusions are drawn:

(1) Increasing the magnetic flux density increases the velocity of fluid flow in both vapor and liquid phases,

hence, improves the circulation of the working fluid in the HP.

(2) The HP maximum and average temperatures are reduced, if the magnetic flux density is increased. Furthermore, it leads to reduce the temperature difference along the HP. Therefore, the presence of magnetic field helps to increase the uniformity of temperature distribution.

(3) The "apparent thermal conductivity" is increased as the magnetic flux density is increased and hence more heat transferring.

(4) Increasing the magnetic flux density is associated with reduction of the operation pressure of the HP, ensuring more safe condition for its operation.

It is worth mentioning that, by reversing the direction of the magnetic field, all the mentioned conclusions get reversed. I.e., the velocity of fluid flow in both vapor and liquid phases is reduced, the HP maximum and average temperatures are increased, the apparent thermal conductivity is reduced, and the operation pressure of the HP is increased.

9. Acknowledgements

References

[1]   D. Reay, R. McGlen, P. Kew, 2013, *Heat pipes: theory, design and applications*, Butterworth-Heinemann,
[2]   A. Faghri, 1995, *Heat pipe science and technology*, Global Digital Press,
[3]   R. Gaugler, Heat transfer device, us patent no. 2350348, applied december 21, 1942, *Published June,* Vol. 6, pp. 1.1, 1994.
[4]   G. Grover, T. Cotter, G. Erickson, Structures of very high thermal conductance, *Journal of applied physics,* Vol. 35, No. 6, pp. 1990-1991, 1964.
[5]   T. Cotter, 1965, *Theory of heat pipes*, Los Alamos Scientific Laboratory of the University of California,
[6]   G. M. Grover, Evaporation-condensation heat transfer device, Google Patents, 1966.
[7]   G. Carbajal, C. Sobhan, G. Peterson, Numerical study of heat pipe heat spreaders with large periodic heat input, *Journal of thermophysics and heat transfer,* Vol. 20, No. 4, pp. 835-841, 2006.
[8]   U. Vadakkan, J. Y. Murthy, S. V. Garimella, Transient analysis of flat heat pipes, in *Proceeding of,* 507-517.
[9]   S. V. Garimella, C. Sobhan, Recent advances in the modeling and applications of nonconventional heat pipes, *Advances in Heat Transfer,* Vol. 35, pp. 249-308, 2001.
[10]   G. J. Carbajal-Benitez, *Analysis of passive two-phase heat dissipation methodologies for high heat flux impingement*, Thesis, Rensselaer Polytechnic Institute, Troy, NY, 2006.
[11]   B. Suman, Modeling, experiment, and fabrication of micro-grooved heat pipes: an update, 2007.
[12]   B. Xiao, A. Faghri, A three-dimensional thermal-fluid analysis of flat heat pipes, *International Journal of Heat and Mass Transfer,* Vol. 51, No. 11-12, pp. 3113-3126, 2008.
[13]   A. Faghri, M. Buchko, Experimental and numerical analysis of low-temperature heat pipes with multiple heat sources, 1991.
[14]   J. Rice, A. Faghri, Analysis of porous wick heat pipes, including capillary dry-out limitations, in *Proceeding of,* 595-607.
[15]   R. Ranjan, J. Y. Murthy, S. V. Garimella, U. Vadakkan, A numerical model for transport in flat heat pipes considering wick microstructure effects, *International Journal of Heat and Mass Transfer,* Vol. 54, No. 1-3, pp. 153-168, 2011.
[16]   A. Faghri, Frontiers in Heat Pipes (FHP), 2014, 5, 1, *Global Digital Central, ISSN*.
[17]   R. J. Hosking, R. L. Dewar, 2016, *Fundamental fluid mechanics and magnetohydrodynamics*, Springer,
[18]   M. Mohammadi, A. Farajpour, A. Moradi, M. Hosseini, Vibration analysis of the rotating multilayer piezoelectric Timoshenko nanobeam, *Engineering Analysis with Boundary Elements,* Vol. 145, pp. 117-131, 2022.

[19]   M. Mohammadi, A. Rastgoo, Primary and secondary resonance analysis of FG/lipid nanoplate with considering porosity distribution based on a nonlinear elastic medium, *Mechanics of Advanced Materials and Structures,* Vol. 27, No. 20, pp. 1709-1730, 2020.

[20]   F. Cingroš, Magnetic Field Control of Heat Transport in Heat Pipes, 2014.

[21]   H. Aminfar, M. Mohammadpourfard, R. Maroofiazar, Experimental study on the effect of magnetic field on critical heat flux of ferrofluid flow boiling in a vertical annulus, *Experimental thermal and fluid science,* Vol. 58, pp. 156-169, 2014.

[22]   X. Wang, Y. Jiao, Study on the heat transfer characteristic of heat pipe containing magnetic nano-fluids strengthened by magnetic field, *Math. Model. Eng. Probl,* Vol. 2, pp. 5-8, 2015.

[23]   S.-W. Kang, Y.-C. Wang, Y.-C. Liu, H.-M. Lo, Visualization and thermal resistance measurements for a magnetic nanofluid pulsating heat pipe, *Applied Thermal Engineering,* Vol. 126, pp. 1044-1050, 2017.

[24]   B. Jeyadevan, H. Koganezawa, K. Nakatsuka, Performance evaluation of citric ion-stabilized magnetic fluid heat pipe, *Journal of magnetism and magnetic materials,* Vol. 289, pp. 253-256, 2005.

[25]   Z. Ming, L. Zhongliang, M. Guoyuan, C. Shuiyuan, The experimental study on flat plate heat pipe of magnetic working fluid, *Experimental thermal and fluid science,* Vol. 33, No. 7, pp. 1100-1105, 2009.

[26]   Y.-C. Chiang, J.-J. Chieh, C.-C. Ho, The magnetic-nanofluid heat pipe with superior thermal properties through magnetic enhancement, *Nanoscale research letters,* Vol. 7, No. 1, pp. 1-6, 2012.

[27]   M. Mohammadi, M. Mohammadi, M. Shafii, Experimental investigation of a pulsating heat pipe using ferrofluid (magnetic nanofluid), *Journal of Heat Transfer,* Vol. 134, No. 1, 2012.

[28]   M. Mohammadi, A. Farajpour, A. Rastgoo, Coriolis effects on the thermo-mechanical vibration analysis of the rotating multilayer piezoelectric nanobeam, *Acta Mechanica*, https://doi.org/10.1007/s00707-022-03430-0, 2023.

[29]   H. Shabgard, A. Faghri, Performance characteristics of cylindrical heat pipes with multiple heat sources, *Applied Thermal Engineering,* Vol. 31, No. 16, pp. 3410-3419, 2011.

[30]   M. Shafahi, V. Bianco, K. Vafai, O. Manca, An investigation of the thermal performance of cylindrical heat pipes using nanofluids, *International journal of heat and mass transfer,* Vol. 53, No. 1-3, pp. 376-383, 2010.

[31]   J. Ramos, N. Winowich, Finite difference and finite element methods for MHD channel flows, *International journal for numerical methods in fluids,* Vol. 11, No. 6, pp. 907-934, 1990.

[32]   R. Rennie, J. Law, 2019, *A dictionary of physics*, Oxford University Press,

[33]   H. KOZAI, H. IMURA, Y. IKEDA, The permeability of screen wicks, *JSME international journal. Ser. 2, Fluids engineering, heat transfer, power, combustion, thermophysical properties,* Vol. 34, No. 2, pp. 212-219, 1991.

[34]   H. Noda, K. Yoshioka, T. Hamatake, An experimental study on the permeability of screen wicks, *JSME International Journal Series B Fluids and Thermal Engineering,* Vol. 36, No. 2, pp. 357-363, 1993.

[35]   S. Ergun, A. A. Orning, Fluid flow through randomly packed columns and fluidized beds, *Industrial & Engineering Chemistry,* Vol. 41, No. 6, pp. 1179-1184, 1949.

[36]   N. Pooyoo, S. Kumar, Numerical Simulation of Cylindrical Heat Pipe Using Al2O3-Water Nanofluid as the Working Fluid, *International Energy Journal,* Vol. 22, No. 3, 2022.

[37]   R. E. Sonntag, G. J. Van Wylen, *Introduction to thermodynamics: classical and statistical*, pp. 1971.

[38]   U. V. Veedu, *Transient three-dimensional modeling of flat heat pipes with discrete heat sources*, Thesis, Purdue University, 2004.

[39]   U. Vadakkan, S. V. Garimella, J. Y. Murthy, Transport in flat heat pipes at high heat fluxes from multiple discrete sources, *J. Heat Transfer,* Vol. 126, No. 3, pp. 347-354, 2004.

[40]   M. M. Heyhat, A. Irannezhad, Experimental investigation on the competition between enhancement of electrical and thermal conductivities in water-based nanofluids, *Journal of Molecular Liquids,* Vol. 268, pp. 169-175, 2018.

[41]   V. Artemov, A. Volkov, A. Pronin, Electrical properties of water: a new insight, *Biophysics,* Vol. 59, No. 4, pp. 520-523, 2014.

[42]   J. G. Collier, J. R. Thome, 1994, *Convective boiling and condensation*, Clarendon Press,

[43]   V. P. Carey, 2020, *Liquid-vapor phase-change phenomena: an introduction to the thermophysics of vaporization and condensation processes in heat transfer equipment*, CRC Press,

[44]   A. Dargys, J. Kundrotas, 1994, *Handbook on physical properties of Ge, Si, GaAs and InP*, Science and Encyclopedia Publishers Vilnius,

[45]   A. I. Zografos, W. A. Martin, J. E. Sunderland, Equations of properties as a function of temperature for seven fluids, *Computer Methods in Applied Mechanics and Engineering,* Vol. 61, No. 2, pp. 177-187, 1987.